Kinetic Analysis of Product Inhibition in Human Manganese Superoxide Dismutase†

Amy S. Hearn,‡ M. Elizabeth Stroupe,§ Diane E. Cabelli,|| James R. Lepock,⊥ John A. Tainer,§ Harry S. Nick,@ and David N. Silverman*,‡

Departments of Pharmacology and Neuroscience, University of Florida, Gainesville, Florida 32610, Department of Molecular Biology, The Scripps Research Institute, 10550 North Torrey Pines Road, La Jolla, California 92037, Department of Chemistry, Brookhaven National Laboratory, Upton, New York 11973-5000, and Department of Physics, University of Waterloo, Waterloo, Ontario N2L3G1, Canada

Received May 22, 2001; Revised Manuscript Received August 9, 2001

ABSTRACT: Manganese superoxide dismutase (MnSOD) cycles between the Mn(II) and Mn(III) states during the catalyzed disproportionation of $O_2^{\bullet-}$, a catalysis that is limited at micromolar levels of superoxide by a peroxide-inhibited complex with the metal. We have investigated the role in catalysis and inhibition of the conserved residue Trp161 which forms a hydrophobic side of the active site cavity of MnSOD. Crystal structures of mutants of human MnSOD in which Trp161 was replaced with Ala or Phe showed significant conformational changes on adjacent residues near the active site, particularly Gln143 and Tyr34 which in wild-type MnSOD participate in a hydrogen bond network believed to support proton transfer during catalysis. Using pulse radiolysis and observing the UV absorbance of superoxide, we have determined rate constants for the catalytic dismutation of superoxide. In addition, the rates of formation and dissociation of the product-inhibited complex of these mutants were determined by direct observation of the characteristic visible absorption of the oxidized and inhibited states. Catalysis by W161A and W161F MnSOD was associated with a decrease of at least 100-fold in the catalytic rate of reduction of superoxide, which then promotes a competing pathway leading to product inhibition. The structural changes caused by the mutations at position 161 led to small changes, at most a 6-fold decrease, in the rate constant for formation of the inhibited complex. Solvent hydrogen isotope effects support a mechanism in which formation of this complex, presumably the peroxide dianion bound to the manganese, involves no rate-contributing proton transfer; however, the dissociation of the complex requires proton transfer to generate HO_2^- or H_2O_2.

Manganese superoxide dismutase (MnSOD)[1] is a homotetramer of 22 kDa subunits that protects mitochondria from oxidative damage associated with electron transport (*1*, *2*). During catalysis, MnSOD cycles between oxidized and reduced forms, resulting in the disproportionation of superoxide (*3*, *4*).

$$\text{Mn(III)SOD} + O_2\cdot^- \rightleftharpoons [\text{Mn(III)SOD-}O_2\cdot^-] \rightarrow \text{Mn(II)SOD} + O_2$$

$$\text{Mn(II)SOD} + O_2\cdot^- + 2H^+ \rightleftharpoons [\text{Mn(II)SOD-}O_2\cdot^-] + 2H^+ \rightleftharpoons \text{Mn(III)SOD} + H_2O_2$$
$$\downarrow\uparrow$$
$$\text{Mn-X-SOD}$$

The first two reactions form a complete catalytic cycle, but the catalysis is complicated by a product-inhibited complex, Mn−X−SOD (*5*−*7*). On the basis of its visible absorbance spectrum, the inhibited complex is suggested to be a side-on peroxo complex resulting from the oxidative addition of superoxide to Mn(II)SOD (*6*). When inhibited in this manner, the decay of superoxide follows zero-order kinetics in a process accompanied by the regeneration of the active enzyme (*6*, *8*). The formation of the inhibited complex of MnSOD is reversible (*7*) and is different from the Fenton chemistry between H_2O_2 and the metals of FeSOD and Cu,-ZnSOD which results in the permanent inactivation of these enzymes (*2*, *9*, *10*).

The focus of this work is on product inhibition with emphasis on site-specific mutations at Trp161 of human wild-type MnSOD, chosen because W161F MnSOD is the most product-inhibited form of MnSOD reported to date (*11*). The side chain of Trp161 forms one hydrophobic side of the active site cavity of MnSOD with the Nϵ of its indole ring 5.6 Å from the metal (Figure 1) (*12*). There is an extensive hydrogen bond network extending into the active site which includes Tyr34, Glu143, His30, and Tyr166 from an adjacent subunit, the manganese-bound solvent molecule, and another water molecule. This hydrogen bond network also appears in FeSOD and may possibly play a role in the catalysis (*13*−*15*).

We report here that replacement of Trp161 with Ala by site-specific mutagenesis caused significant conformational changes of the side chains of Gln143 and Tyr34 near the active site, determined from the crystal structure. We have estimated the rate constants for formation and dissociation

† This work was supported by National Institutes of Health Grants GM54903 (to D.N.S.), GM48495 (to J.A.T.), and HL39593 (to H.S.N.). Pulse radiolysis studies were carried out at the Center for Radiation Chemical Research at BNL, which is supported under Contract DE-AC02-98CH10886 with the U.S. Department of Energy and supported by its Division of Chemical Sciences, Office of Basic Energy Sciences.

* To whom correspondence should be addressed: Box 100267, Health Center, University of Florida, Gainesville, FL 32610-0267. Phone: (352)392-3556. Fax: (352)392-9696. E-mail: silvrmn@nervm.nerdc.ufl.edu.

‡ Department of Pharmacology, University of Florida.

§ The Scripps Research Institute.

|| Brookhaven National Laboratory.

⊥ University of Waterloo.

@ Department of Neuroscience, University of Florida.

[1] Abbreviations: MnSOD, manganese superoxide dismutase; W161A MnSOD, site-specific mutant of MnSOD with Trp161 replaced with Ala; SHIE, solvent hydrogen isotope effect; Ches, 2-(cyclohexylamino)-ethanesulfonic acid; Mops, 3-(*N*-morpholino)propanesulfonic acid; Taps, 3-[tris(hydroxymethyl)methyl]aminopropanesulfonic acid.

10.1021/bi011047f CCC: $20.00
Published on Web 09/13/2001

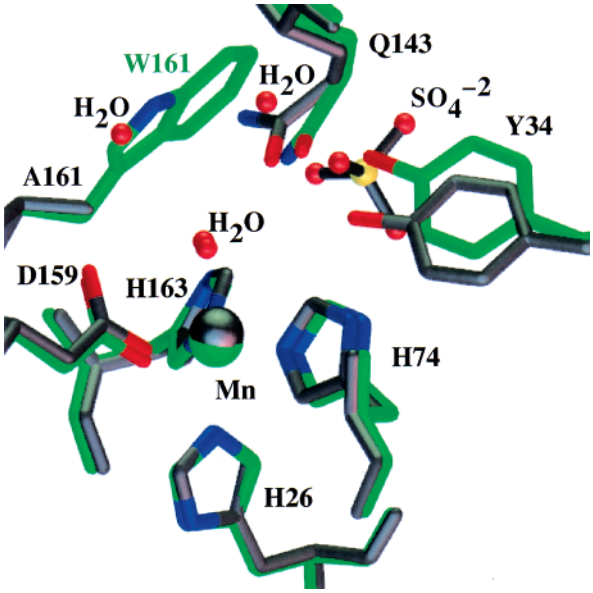

FIGURE 1: Structure of the active site of human W161A MnSOD (gray) superimposed on that of wild-type human MnSOD [green; data from Borgstahl et al. (*12*)].

of the product-inhibited complex by direct observation of characteristic visible absorptions for the free, oxidized enzyme and for the inhibited complex formed during catalysis. Catalysis was initiated by production of superoxide by pulse radiolysis. The data emphasize the role of the competition between catalysis and the steps leading to inhibition, with the mutations at position 161 decreasing catalysis and promoting inhibition. The structural changes caused by the mutations at position 161 led to surprisingly little change in the rate constant for formation of the inhibited complex. Solvent hydrogen isotope effects support a mechanism in which formation of this complex, presumably the peroxide dianion bound to the manganese, involves no rate-contributing proton transfer; however, the dissociation of the complex requires proton transfer to generate HO_2^- or H_2O_2.

METHODS

Preparation and Purification of Enzymes. The human MnSOD cDNA [cDNA sequence determined by Beck et al. (*16*)] was amplified by PCR using the oligonucleotides GCATATGAAGCACAGCCTCC and GGAGATCTCAGCATAACGATC as primers. The plasmid pHMNSOD4 (ATCC 59947) containing human MnSOD was subcloned into the TA cloning vector pCRII (Invitrogen Corp.). Four primers were used to generate the mutants W161X (X = A, F, H, V, or Y), H30N, and Y34F. The first pair of oligonucleotides was the same for all of the mutants and was used to regenerate the entire coding region: primer 1, 5′-CGCTAGTAATCATTTCATGAAGCACAGCCTCCCCG-3′; and primer 2, 5′-CGCCAAAACAGCCAAGCTTTCATGCTCGCAG-3′. The second pair of oligonucleotides (designated primers 3 and 4) were complementary internal primers which encoded the mutation of interest (underlined). The following primers were used: W161 primer 3, 5′-GGGATTGATGTGTGGGAGCATGCTTAC-3′; and W161 primer 4, 5′-GTAAGCATGCTCCCACACATCAATCCC-3′; H30 primer 3, 5′-CAGCTGCACCATTCGAAGCACCACGCGGCCTA-3′; and H30 primer 4, 5′-TAGGCCGCGTGGTGCTTCGAATGGTGCAGCTG-3′; and Y34 primer 3, 5′-CCACGCGGCCTACGTTAACAACCTG-3′; and Y34 primer 4, 5′-CAGGTTGTTAACGTAGGCCGCCGTGG-3′. The 5′ half of the coding sequence was amplified using primers 1 and 4, while a second reaction using primers 2 and 3 generated the 3′ half of the MnSOD coding sequence. A second round of PCR was performed using the products from the first two reactions (purified by electroelution) as templates with primers 1 and 2. The restriction sites *Bsp*HI and *Pst*I (incorporated into primers 1 and 2, respectively) were used for cloning the PCR products into the expression vector pTrc 99A (Pharmacia Corp.). The *Bsp*HI site, which is located in the N-terminal portion of the protein, was annealed to the compatible cohesive ends of the *Nco*I site in pTrc 99A, regenerating an ATG codon. *Pst*I was used to cut and anneal the C-terminal end of the cDNA to pTrc 99A. DNA sequencing was used to verify the coding sequence, including the new mutation. The plasmid was then transformed into the *Escherichia coli* (strain QC774) *Sod A*$^-$*/Sod B*$^-$ null mutant (*17*), where it expressed human MnSOD as a mature protein tagged with an extra methionine at the amino terminus. The bacterial medium included 660 μM $MnCl_2$. Yields of human MnSOD mutant protein were approximately 70 mg of protein/50 g of bacterial pellet.

Mutant human MnSOD enzymes were purified from *E. coli* by utilizing heat treatment (60 °C), dialysis (against the appropriate buffer with EDTA), and ion exchange chromatography (DE52 and CM52) according to the procedures previously described (*18*). SDS−polyacrylamide gels were used to visualize the final purity of the samples. The gels exhibited one intense band at ∼22 kDa, indicative of the monomer. After extensive dialysis, the metal content of each of the samples was determined by atomic absorption spectroscopy. The manganese concentration was used in all of our calculations as the concentration of the active enzyme. Protein concentrations were determined by the Lowry method; the ratio of manganese concentration to total protein concentration varied from 0.40 for W161V to 1.00 for W161Y.

Pulse Radiolysis. The pulse radiolysis experiments were performed at Brookhaven National Laboratory using a 2 MeV van de Graaff accelerator. A path length of either 2.0 or 6.1 cm was used for all experiments. All UV−vis spectra were measured on a Cary 210 spectrophotometer at 25 °C. Dosimetry was defined with the KSCN dosimeter, assuming that $(SCN)_2^-$ has a *G* value of 6.13 and a molar absorptivity of 7950 M^{-1} cm^{-1} at 472 nm (*19*). The measured rate constants are based on the manganese concentration from atomic absorption spectroscopy and not on the protein concentration. All of the metal present is presumed to be bound in the active site and functioning independently of the other metal centers. Solutions were made in H_2O or D_2O and contained enzyme and 30 mM sodium formate [as a hydroxyl radical scavenger (*20*)], 50 μM EDTA, and 2 mM buffer [Mops (pH 6.5−7.25), Taps (pH 7.5−9.25), or Ches (pH 9.5−10.5)]. Superoxide radicals (1−30 μM) were formed by exposing aqueous, air-saturated solutions to a high-dose electron pulse. In a solution containing formate and O_2, the primary radicals (OH, e_{aq}^-, and H) created by the electron pulse are converted to superoxide by a number of scavenging reactions discussed by Schwarz (*20*). In these experiments, $O_2^{\bullet-}$ formation is more than 90% complete within 1 μs of the pulse. The reactions were monitored

Table 1: Transition Temperatures for the Unfolding of Wild-Type Human MnSOD and Mutants at Position 161

residue at position 161	T_m (°C)[a]	residue at position 161	T_m (°C)[a]
Phe	96.0	Trp (wild type)	88.9[b]
His	96.0	Val	85.1
Ala	89.8	Tyr	83.3

[a] The estimated standard deviation in values of T_m was ~0.2 °C arising from multiple scans of a single enzyme sample. [b] From Guan et al. (*13*).

spectrophotometrically following changes in the absorbance of superoxide (*21*) or enzyme (*11*). Repeated pulse radiolysis experiments on the same enzyme sample gave superimposable kinetic traces; the pulse radiolysis itself did not alter the catalytic properties of the enzymes used here.

Solvent hydrogen isotope effects (SHIEs) were determined by measuring the ratio of rate constants (under the same conditions) in H_2O and D_2O (>0.98 atomic fraction deuterium). Uncorrected pH meter readings are reported. This relies on the fact that the correction of a pH meter reading in 100% D_2O is approximately offset by the change in ionization constant of nearly all acids with values of pK_a within the pH range of this study (*22*). Kinetic solvent isotope effects for the catalyzed dismutation of superoxide were measured at pH 8.2, a value for which measured kinetic constants exhibit no or very little change with small variations in pH.

Differential Scanning Calorimetry. A CSC Nano high-sensitivity differential scanning calorimeter was used to obtain all denaturation profiles. Human MnSOD and the W161 mutants at 1.0 mg/mL in 20 mM potassium phosphate buffer (pH 7.8) were degassed under mild vacuum for 5 min and immediately scanned at a rate of temperature increase of 1 °C/min. The baseline and change in specific heat (ΔC_p) upon denaturation were corrected as described previously (*23*). Essentially, the baseline immediately preceding the transition and that following it were assumed to be linear, and the baseline under the transition was taken as an average of the two baselines weighted for the fraction of the transition completed. The peaks of the differential scanning calorimetry profile were deconvoluted assuming a reversible, non-two-state model using the software package ORIGIN (Microcal, Inc.). ΔH, ΔS, and T_m for each transition were obtained from the best fits. The T_m values in Table 1 are the temperatures at which C_p reached a maximum.

Crystallography. Crystals of W161A human MnSOD were grown from 2−3 M ammonium sulfate in 100 mM imidazole/malate buffer at pH 7.5−8 and belonged to space group $P6_122$ with the following unit cell dimensions: $a = 79.6$ Å, $b = 79.6$ Å, and $c = 240.1$ Å. A single crystal was used, frozen in a stream of liquid nitrogen protected by 20% ethylene glycol in the well solution. Data to 2.1 Å resolution were collected at the Stanford Synchotron Radiation Laboratory on beamline 9-1 with 0.77 Å radiation and a MAR-345 scanner and processed using Scalepack and DENZO (*24*). Overall, the data were 98.9% complete (100% in the lowest bin) with an R_{symm} of 5.7% (42.7% in the highest-resolution bin). The I/σ value was 9.8, and in the highest-resolution bin, it was 4. The protein structure was determined by rigid body refinement of the W161A data against the wild-type structure. Successive rounds of Powell minimizations and *B*-factor refinement were performed using CNS, and maps ($2F_o - F_c$ and $F_o - F_c$) were fit with the Xfit suite (*25*), to bring the final R_{cryst} to 24.9% and R_{free} to 28.9%. Coordinates have been deposited in the Protein Data Bank as entry 1JA8.

RESULTS

Crystal Structures. Superposition of the structure of human W161A MnSOD with that of wild-type MnSOD (*12*) showed that the overall structures of these enzymes are nearly identical, and very similar to that of the previously crystallized mutant W161F (Figure 2 of ref *11*). The root-mean-square deviation between the Cα's of the mutant W161A and the wild type is 0.17 Å. The positions of the four amino acid ligands of the manganese (His26, His74, His163, and Asp159) form a strained trigonal bipyramidal coordination in W161A that is very closely superimposable with that of the wild type (Figure 1). It was observed for W161A MnSOD that new water molecules fill the cavity created when this active site residue is replaced with Ala. Similar observations of new water molecules in mutant structures were made with human Q143A (*26*) and Q143N MnSOD (*23*). One of the new water molecules in W161A approximates the position of Nϵ of W161 in the wild type and forms a hydrogen bond with the manganese-bound water (heavy atom distance of 2.9 Å) and also with the side chain of Gln143 (2.9 Å) (Figure 1). The side chain of Gln143 in W161A forms another hydrogen bond with the manganese-bound water (3.1 Å), but this hydrogen bond is weaker than its counterpart in the wild type (2.9 Å). In the wild type, the side chains of Gln143 and Tyr34 are hydrogen bonded and form part of an extended hydrogen bond network that also includes His30 and Tyr166 (*12*). In the structure of W161A MnSOD, Gln143 rotates slightly to accommodate the smaller volume of Ala instead of Trp at position 161, placing its Nϵ within hydrogen bonding distance of the manganese-bound solvent molecule, as mentioned above, and ~4.0 Å away from the hydroxyl of Tyr34 which moves quite significantly from its position in the wild-type enzyme (Figure 1). In W161A MnSOD the distance between the amide group of Gln143 and the hydroxyl of Tyr34 is too great (4.0 Å) to form a hydrogen bond. Hence, W161A interrupts the hydrogen bond network, as do a number of other active site mutations reported previously (*13*, *26*, *27*).

In the mutant W161A MnSOD, a single sulfate molecule is bound at the dimer interface formed by crystallographic symmetry in the cavity that remains after removing W161 (Figure 1). Two oxygens of this sulfate molecule approximate the positions of two water molecules in the wild-type enzyme. It is bound by hydrogen bonds with Tyr34, His30, and several water molecules. A shift in Tyr34 seems to occur in response to the changes in Gln143 and to accommodate the sulfate molecule. With the sulfate bound, Tyr34 has rotated, moving the phenolic oxygen approximately 2.2 Å from its wild-type position and breaking the hydrogen bond with Gln143, as mentioned above. For residues more distant from the metal, such as His30, there is no appreciable difference in side chain conformation compared with that of the wild type, despite a hydrogen bond (2.8 Å) between the side chain Nδ of His30 and an oxygen of the sulfate.

Thermal Stability. Differential scanning calorimetry was used to determine the thermal stability of the human wild-type MnSOD and variants at position 161 (Table 1). Modest

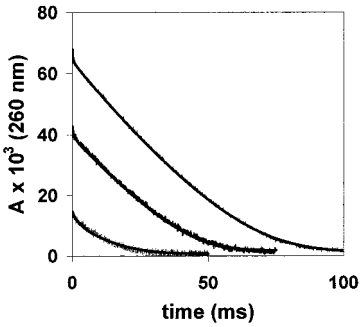

FIGURE 2: Decrease in the absorbance of superoxide at 260 nm in the presence of 1 μM W161A MnSOD measured by pulse radiolysis. Solutions contained 30 mM formate, 50 μM EDTA, and 2 mM TAPS at pH 8.2 and 25 °C. Initial concentrations of superoxide were (from top to bottom) 17.1, 10.1, and 3.3 μM. The solid lines are a fit of the McAdam mechanism (eqs 1−4) with the following values: $k_1 = (8.0 \pm 0.2) \times 10^7$ M^{-1} s^{-1}, $k_2 < 1 \times 10^7$ M^{-1} s^{-1}; $k_3 = (3.8 \pm 0.2) \times 10^8$ M^{-1} s^{-1}, and $k_4 = 140 \pm 11$ s^{-1}. The value of the zero-order rate constant k_0/[E] for the 17.1 μM trace (top) was 450 s^{-1}.

changes were found in the main unfolding transition, with W161F being the most stable with a 7.1 °C increase in T_m and W161Y the least stable with a 5.6 °C decrease in T_m compared with that of the wild type. W161F and W161Y differ only by one hydroxyl group, but this structural change results in a 12.7 °C change in T_m, suggesting major changes in hydrogen bonding between these mutant enzymes. All of the mutants at position 161 listed in Table 1 have values within 7 °C of that of the wild-type enzyme (89 °C). The structural changes observed between the wild-type enzyme and the W161A mutant have almost no effect on thermal stability (Table 1). The unfolding transition, which is a measure of conformational stability, is different from the thermal inactivation temperature which is 70 °C for human wild-type MnSOD and is due to a much smaller conformational change for thermal inactivation than for unfolding (*13*). We attempted to prepare other mutants with replacements at position 161, such as W161L; however, these were not stable enough to isolate.

Observation of the Absorbance of Superoxide. Superoxide was rapidly created by pulse radiolysis (~1 μs) in solutions containing dissolved oxygen. The decrease in the absorption of superoxide was followed at 260 nm as a function of time to measure the rate of the catalytic disappearance of superoxide in the presence of wild-type MnSOD and mutants. At an initial concentration of $O_2^{\bullet-}$ of 3.3 μM, the decay of superoxide catalyzed by 1 μM W161A MnSOD appeared to be a predominantly first-order process; at an initial concentration of $O_2^{\bullet-}$ of 17.1 μM, there was a predominant contribution of a zero-order component (Figure 2). This behavior at the higher superoxide concentration is similar to that described for human wild-type MnSOD (*8*) and attributed to a product inhibition as seen in bacterial MnSODs (*5*, *6*).

To fit kinetic data for catalysis by MnSOD from *Bacillus stearothermophilus*, McAdam et al. (*5*) proposed a simplified mechanism (eqs 1−4) in which individual steps are considered irreversible, justified in part by the favorable equilibrium constants associated with eqs 1 and 2. Equations 3 and 4 represent the formation and dissociation of the product-inhibited complex.

$$\text{Mn(III)SOD} + O_2^{\bullet-} \xrightarrow{k_1} \text{Mn(II)SOD} + O_2 \quad (1)$$

$$\text{Mn(II)SOD} + O_2^{\bullet-} \xrightarrow{k_2\,(+2H^+)} \text{Mn(III)SOD} + H_2O_2 \quad (2)$$

$$\text{Mn(II)SOD} + O_2^{\bullet-} \xrightarrow{k_3} \text{Mn}-\text{X}-\text{SOD} \quad (3)$$

$$\text{Mn}-\text{X}-\text{SOD} \xrightarrow{k_4\,(+2H^+)} \text{Mn(III)SOD} + H_2O_2 \quad (4)$$

The advantage of this scheme for this work is that it simplifies the catalytic cycle of eqs 1 and 2 while emphasizing the formation and dissociation of the Mn−X−SOD inhibited complex in eqs 3 and 4. Further implications of this scheme appear in the Discussion. The role of protonation in catalysis is indicated in eqs 2 and 4 and is a topic of this work. The source of the protonation is uncertain and could be solvent water, water as a ligand of the metal, or ionizable groups on the enzyme itself.

Progress curves such as shown in Figure 2 were analyzed by fitting to the data this simplified model of catalysis (eqs 1−4) and the known second-order rates of the uncatalyzed dismutation. We used two fitting programs, PRKIN[2] and FITSIM (*28*), which are based on the numerical solution of the simultaneous kinetic equations; both gave the same results. To reduce the range of solutions that fit the data such as shown in Figure 2, we fixed k_3 and k_4 at the values shown in Table 2 determined, as described below, by direct observation of the characteristic absorbances of the oxidized enzyme and inhibited complex; the fitting programs were then used to obtain the values of k_1 and k_2. With this procedure, we were able to determine values of k_1. The values of k_2 were small compared with k_1 and k_3 for catalysis by W161A and W161F and allowed us to determine only an upper limit for k_2 (Table 3). Because of the similar values of k_2 and k_3 for wild-type MnSOD, we were not able to differentiate these rate constants, and the value represented in Table 3 is the sum $k_2 + k_3$. Table 3 also gives the values of the zero-order rate constant k_0/[E_0] determined by a fit of data such as shown in Figure 2, including a zero-order decay of $O_2^{\bullet-}$ observed at 260 nm.

Observation of the Absorbance of the Free and Inhibited Enzyme. The rate constants k_3 and k_4 that measure the formation and dissociation of the product-inhibited complex, (eqs 3 and 4), were determined from the absorption maxima of MnSOD and mutants and their inhibited complexes. The free enzyme W161A Mn(III)SOD is characterized by an absorption at 480 nm (Figure 3, inset) ($\epsilon_{480} = 600$ M^{-1} cm^{-1} for human MnSOD) (*7*); in the reduced state, Mn(II)SOD has only a very small visible absorption (ϵ_{420}, $\epsilon_{480} < 30$ M^{-1} cm^{-1}). The inhibited complex is characterized by a significant absorption at 420 nm shown in the inset of Figure 3 for W161A MnSOD ($\epsilon_{420} = 500$ M^{-1} cm^{-1} for human MnSOD) (*7*). W161A MnSOD was reduced with H_2O_2 before single-turnover experiments in which $O_2^{\bullet-}$ was generated by pulse radiolysis. Figure 3 shows typical data for the first-order increase in absorption at 420 nm as the inhibited complex accumulated. Estimation of the concentration of the inhibited complex at the plateau, based on the ϵ_{420} given above, shows all of the $O_2^{\bullet-}$ introduced by pulse radiolysis had been

[2] H. A. Schwarz, unpublished program.

Table 2: Rate Constants for the Formation (k_3) and Dissociation (k_4) of the Inhibited Complex and Their Solvent Hydrogen Isotope Effects for Human Wild-Type MnSOD and Site-Specific Mutants[a]

enzyme	k_3 (nM^{-1} s^{-1})	k_4 (s^{-1})	$^{D}k_3$[b]	$^{D}k_4$[b]
wild type	1.1 ± 0.1[c]	117 ± 5	1.2 ± 0.2	1.7 ± 0.2
W161A	0.37 ± 0.04	180 ± 20	1.1 ± 0.1	2.3 ± 0.6
W161F	0.46 ± 0.04	33 ± 3	1.0 ± 0.1	2.2 ± 0.2
W161V	0.27 ± 0.01	265 ± 16	1.2 ± 0.1	2.0 ± 0.3
W161Y	0.20 ± 0.01	130 ± 10	1.2 ± 0.1	1.9 ± 0.2
W161H	0.29 ± 0.03	136 ± 7	1.1 ± 0.1	1.8 ± 0.3
Y34F	0.49 ± 0.09	56 ± 4	1.1 ± 0.1	2.0 ± 0.2
H30N	0.68 ± 0.02	500 ± 130	1.5 ± 0.1	1.7 ± 0.5

[a] Measured at pH 8.2 and 25 °C with other conditions as described in the legend of Figure 3. [b] $^{D}k_3$ is the solvent hydrogen isotope effect on this constant, $(k_3)_{H_2O}/(k_3)_{D_2O}$. Similarly for $^{D}k_4$. [c] This value represents $k_2 + k_3$; due to similar magnitudes for k_2 and k_3, we could not determine these constants individually. See the text.

Table 3: Rate Constants (eqs 1 and 2) for Catalysis by Human MnSOD and the Zero-Order Rate Constant Resulting from Product Inhibition[a]

enzyme	k_1 (nM^{-1} s^{-1})	k_2 (nM^{-1} s^{-1})	$k_0/[E_0]$ (s^{-1})
wild type	1.5 ± 0.1	1.1 ± 0.1[b]	500[c]
W161F	0.30 ± 0.08	<0.01	50[c]
W161A	0.08 ± 0.02	<0.01	450

[a] These values were determined by a fit to the decrease of the superoxide absorbance at 260 nm, such as shown in Figure 2, using PRKIN[2] and FITSIM (*28*), both of which gave the same results within the indicated ranges of standard errors. Conditions as described in the legend of Figure 2. In this fit, k_3 and k_4 were fixed to the values determined directly from the enzyme absorbances given in Table 2. The range of errors indicates the breadth of solutions determined in the fitting programs. [b] This value represents $k_2 + k_3$; due to similar magnitudes for k_2 and k_3, we could not determine these constants individually. See the text. [c] From Cabelli et al. (*11*).

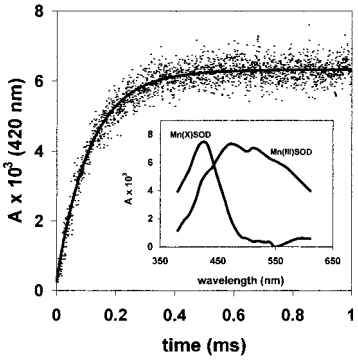

FIGURE 3: Increase in the absorbance at 420 nm of 25 μM W161A MnSOD at short times after pulse radiolysis generated an initial superoxide concentration of 4.9 μM. Solutions in H_2O contained 30 mM formate, 50 μM EDTA, and 2 mM TAPS at pH 8.2. The enzyme had been reduced prior to the experiment with 200 μM H_2O_2. The solid line is a fit to a first-order process with the resulting value of k_3 given in Table 2. The inset shows the visible spectra of W161A Mn(III)SOD and the inhibited complex of W161A MnSOD at the same pH.

converted to the inhibited form of the enzyme. Since we started with the reduced enzyme, we did not observe the pathway described by eq 1. We have found that for W161A and W161F MnSOD, $k_2 \ll k_3$ (compare Tables 2 and 3). Hence, the increase at 420 nm effectively represents k_3,[3] with little contribution from k_2 of eq 2. Values of k_3 were determined in this manner for a series of mutants at position 161 and are presented in Table 2 along with a comparison

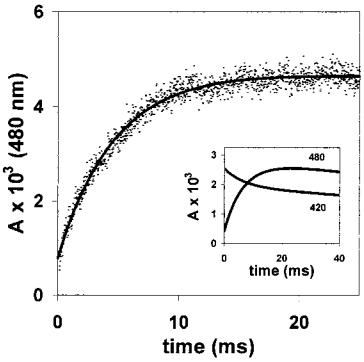

FIGURE 4: Increase in the absorbance at 480 nm of 25 μM W161A MnSOD at longer times after pulse radiolysis generated an initial superoxide concentration of 4.9 μM. Conditions were as described in the legend of Figure 3. The inset shows changes in absorbance at 480 and 420 nm of 25 μM W161A MnSOD upon exposure to 1.7 μM superoxide. Other conditions were as described in the legend of Figure 3. The solid line at 480 nm is a first-order fit with a k_4 of 180 ± 20 s^{-1}. The solid line at 420 nm is a first-order fit with a k_4 of 150 ± 20 s^{-1}.

to values determined for H30N and Y34F MnSOD, the subject of previous reports (*13*, *27*). The data of Table 2 demonstrate a surprisingly small variation in k_3 among these active site mutants.

In an extension of the same experiment, Figure 4 shows the first-order increase in the 480 nm absorption due to the decay of the inhibited complex (eq 4). This demonstrates, under our conditions, the long separation in time between the formation of inhibited complex, complete by 0.4 ms (Figure 3), and its decay, complete in 10 ms (Figure 4). The increase at 480 nm, characteristic of the emergence of the oxidized enzyme (Figure 4), is mirrored by the decrease at 420 nm (Figure 4, inset); overlap of the spectra of W161A Mn(III)SOD and the inhibited form at 420 nm makes the magnitude of the change at 420 nm less than at 480 nm (Figure 4, inset). A value for k_4 of 180 ± 20 s^{-1} was obtained by a first-order fit to the increase at 480 nm (Figure 4) and is given in Table 2; the first-order rate constant from a fit to the decay of the inhibited form at 420 nm (Figure 4, inset) was in agreement with a k_4 of 150 ± 20 s^{-1}. These values are also in agreement with the value for k_4 of 140 ± 11 s^{-1} determined by fitting the catalytic decay of superoxide as described in the legend of Figure 2.

Among the mutants in Table 2, there is a greater variation in k_4, at most 15-fold, than we observed for k_3. Two mutants noted in previous reports to be particularly inhibited, W161F (*11*) and Y34F MnSOD (*13*), have the smallest values of k_4 which are decreased 2−3-fold compared with that of the wild type.

The pH profile of k_3 for W161A MnSOD and $k_2 + k_3$ for the wild type[3] were found to have a significant pH dependence at pH >9.0 for the wild type and at pH >8.0 for the W161A mutant (Figure 5). The pH profile for W161A could be fit to a single ionization with a pK_a of 9.2 ± 0.1. The rate constant k_4 for the dissociation of the inhibited complex with the wild-type enzyme was independent of pH over the

[3] For wild-type MnSOD, the value represented as k_3 in the text and Table 2 is $k_2 + k_3$. These rate constants k_2 and k_3 were similar in magnitude; the measured increase in absorbance at 420 nm represents $k_2 + k_3$ due to overlapping absorbances of Mn(III)SOD and the Mn−X−SOD inhibited complex.

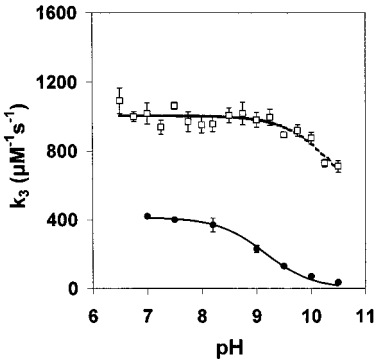

FIGURE 5: pH profile for the rate constant $k_2 + k_3$ for wild-type human MnSOD (□) and k_3 for W161A human MnSOD (●) (eqs 2 and 3). Solutions at 25 °C in H_2O contained 30 mM formate, 50 μM EDTA, 25 μM enzyme, 200 μM H_2O_2, and one of the following buffers (2 mM): Mops (pH 6.5−7.25), Taps (pH 7.5−9.25), or Ches (pH 9.5−10.5). Superoxide concentrations were between 1.0 and 2.5 μM. Data are the means and standard deviations of 5−10 traces. The data for W161A could be fit to a single ionization with a pK_a value of 9.2 ± 0.1.

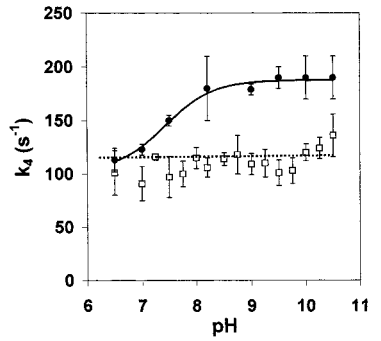

FIGURE 6: pH profile for the rate constant k_4 (eq 4) for wild-type human MnSOD (□) and W161A human MnSOD (●). Conditions were as described in the legend of Figure 6. The data for W161A could be fit to a single ionization with a pK_a of 7.4 ± 0.1.

pH range shown in Figure 6 with a k_4 of 110 ± 10 s^{-1}; however, the W161A mutant exhibited a significant pH dependence of k_4 with a pK_a value of 7.4 ± 0.1 (Figure 6).

The solvent hydrogen isotope effects (SHIEs) determined for k_3 and k_4 show uniform behavior for wild-type MnSOD and the mutants at position 161 as well as for Y34F MnSOD (Table 2). That is, the SHIE on k_3 is unity and that on k_4 is near 2 (Table 2). The SHIEs for catalysis by H30N are similar within experimental error, but show a somewhat increased SHIE for k_3 (Table 2).

DISCUSSION

We have carried out kinetic measurements of superoxide dismutation catalyzed by a series of site-specific mutants at Trp161 of human MnSOD. Our goal is to elucidate the steps involved in product inhibition during catalysis, and this site was chosen because previous work had demonstrated that the mutant in which Trp161 is replaced with Phe is very product-inhibited compared with the wild type (*11*). As shown in Figure 1, the replacement of Trp161 with Ala caused significant variations in the conformations of the side chains of Gln143 and Tyr34, the two side chains of an extensive hydrogen bond network closest to the metal-bound water (this network includes the aqueous ligand of Mn, Gln143, Tyr34, His30, Tyr166, and water molecules) (*12*). To understand more fully this effect, we have compared the

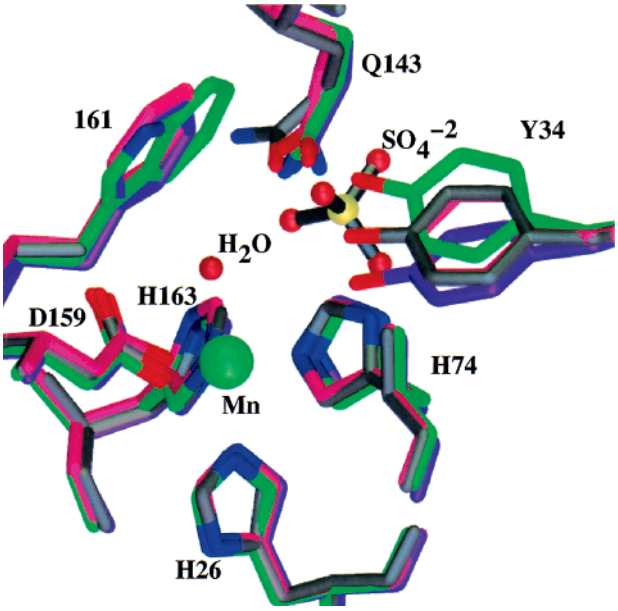

FIGURE 7: Structure of the active site of wild-type human MnSOD (green) superimposed on that of W161F [pink, no sulfate used; from Cabelli et al. (*11*)], W161F (purple, with sulfate),[4] and W161A (gray, this work, with sulfate). The sulfate groups for W161A and W161F are nearly superimposable, and only W161A is shown for clarity.

structures in this region for different variants of human MnSOD. Figure 7 compares the structure of wild-type MnSOD with that of W161A and W161F crystallized in the presence and absence of sulfate.[4] Most apparent from this comparison is the variation in side chain conformations of Gln143 and Tyr34. It appears that one function of Trp161 is to constrain the orientations of Gln143 and Tyr34 for participation in the hydrogen bond network. In W161A MnSOD, there is no hydrogen bond between Gln143 and Tyr34. This active site structure is important in maintaining the redox potential as well as the maximum velocity of catalysis (*23*, *26*).

In terms of contributions to stability, the wild-type enzyme and the variants at position 161 showed modest differences (Table 1), with changes in the major unfolding transition spanning ~7 °C above and below the value of 89 °C for the wild type. The thermal stabilities of wild-type and W161A MnSOD are nearly identical for this transition. The replacement of Trp161 with Phe or His stabilizes the enzyme, while the replacement by Tyr results in the smallest stability. The hydroxyl of the Tyr appears to be destabilizing, while the phenyl ring at this site is stabilizing. These results are consistent with the hypothesis that Trp161, conserved in the MnSODs, was not selected to confer thermostability for this major unfolding, but to maintain an active site environment suitable for catalysis.

The impact on catalysis of the very significant structural changes we made at position 161 was investigated by pulse radiolysis in single-turnover experiments and analyzed by a simplified mechanism for catalysis (eqs 1−4). The most significant effect of the replacement of Trp161 with either Phe or Ala is the decrease by at least 2 orders of magnitude in k_2, accompanied also by substantial although smaller decreases in k_1 (Table 3). In previous work (*23*), changes in

[4] M. E. Stroupe, unpublished observations.

the position of the amide group of Gln143 through mutation to Asn and introduction of a new water molecule in Q143N MnSOD resulted in a significant increase in the redox potential of the active site. We suggest that in W161A MnSOD the changes at position 161 and the change in conformation of Gln143 allowing introduction of new water molecules have also altered the redox potential at the active site. The superoxide dismutases have their redox potentials tuned to be between those of the catalyzed half-reactions of superoxide oxidation and reduction (*3*, *29*), and the data suggest that replacements at position 161 have altered the redox properties of the active site. Any mutation that significantly alters the redox potential of the enzyme out of this range will have a decreased rate of catalysis. W161A and W161F MnSOD are able to oxidize $O_2^{\bullet-}$ with values of k_1 reduced 20-fold for W161A and 5-fold for W161F (Table 3), but the values of k_2 for the catalytic reduction of superoxide by these mutants were smaller by at least 2 orders of magnitude.

In the wild-type human MnSOD, k_2 and k_3 appear to be similar in magnitude. That is, there is evidence for a competition between these two pathways resulting in an intermediate extent of product inhibition, intermediate between those of the extensively inhibited W161F and the slightly inhibited H30N mutants (*27*). The result is a degree of product inhibition in the wild type described in previous reports as occurring on average after several cycles of oxidation and reduction of the uninhibited pathway of eqs 1 and 2 (*6*, *8*). However, with W161F, the pathway very much favors eq 3 leading into the inhibited state. This was a conclusion of Cabelli et al. (*11*) based on pulse radiolysis data for W161F MnSOD which showed no catalytic cycles but rather a pathway that led directly to the inhibited complex.

The significant product inhibition for the position 161 mutants cannot be attributed to any single step, but is a complex process represented by decreases in all of the rate constants for the simplified mechanism of eqs 1−4. However, among these, the very low values of k_2, by orders of magnitude compared with that of wild type, appear to be particularly significant. By decreasing k_2, the presence of Ala161 or Phe161 has favored the formation of the inhibited pathway. That is, the replacement of Trp161 with Ala or Phe has altered the gating between the pathways of catalysis (eqs 1 and 2) and inhibition (eqs 3 and 4). The values described, for example, in the legend of Figure 2 accurately simulate progress curves for W161A MnSOD. Although k_2 is decreased greatly in the position 161 variants, the values of k_3 and k_4 are altered to a much smaller extent (Table 2). Hence, the formation (k_3) and dissociation (k_4) of this inhibited complex are not as sensitive to these changes in the active site as is k_2. No correlations were found between the hydrophobicity at position 161 and the values of k_3 and k_4.

The values of the solvent hydrogen isotope effect (SHIE) give a rather consistent picture for all of the position 161 variants shown in Table 2. That is, the SHIE on k_3 was unity, indicating no change in covalent binding to hydrogen in a rate-contributing step that leads to formation of the inhibited complex. But there was a SHIE near 2 on k_4 for wild-type MnSOD and all of the mutants in Table 2, consistent with a primary proton transfer in the dissociation of the inhibited complex. Overall, the SHIE data are consistent with the formation of a peroxo complex of the metal which occurs with no rate-contributing proton transfer. It is intriguing that the very significant alterations caused by the replacement of Trp161 with Ala, including the altered conformations of active site residues Gln143 and Tyr34, have only minor effects on the rate constant for formation of the product-inhibited complex k_3 (Table 2). This suggests that the formation of this complex is to a considerable extent a function of the metal. However, it is a proton transfer step (or steps) which appears to determine the lifetime of this complex, determined by k_4 of eq 4.

Proposals for the formation of the inhibited complex are reviewed by Cabelli et al. (*4*). Changes in the visible absorption spectrum of the enzyme in the inhibited state suggest an inner sphere coordination of a form of product peroxide (*6*, *7*). The SHIE of unity on k_3 emphasizes that this complex forms without rate-contributing proton transfer, consistent with an inner sphere complex of peroxide dianion O_2^{2-} with manganese, possibly a side-on peroxo complex as suggested by Bull et al. (*6*). A prominent theme of previous considerations of this catalysis is that a role for the hydrogen bond network in the active site is to support proton transfer to form the hydroperoxide anion HO_2^- or H_2O_2 (*14*, *23*, *30*). Replacement of Trp161 or Tyr34 with subsequent changes in active site conformations does have an effect on k_4 with the two most inhibited variants W161F and Y34F MnSOD having the smallest values of k_4 (Table 2).

The rate constant k_3 for formation of the inhibited complex in W161A MnSOD exhibited a pH dependence from which we estimate a pK_a of 9.2 ± 0.1 (Figure 5). The source of this ionization is unknown, although it may relate to the pK_a of the aqueous ligand of the manganese. The level of catalysis by wild-type MnSOD decreases at pH >9 perhaps due to formation of an additional hydroxyl ligand of the metal (*30*, *31*). The data depicted in Figure 6 show that whereas k_4 for the wild type is pH-independent, k_4 for W161A MnSOD exhibits a modest pH dependence at pH <8 (Figure 6). It appears that the donor of a proton to the inhibited complex allowing it to dissociate product is influenced by an ionization with a pK_a of <8 in the mutant.

The simplified mechanism (eqs 1−4) has allowed us to fit adequately the observed catalyzed decay of $O_2^{\bullet-}$ as well as the formation and decay of the product-inhibited complex. A more extensive model, including the reverse reactions, has been used to interpret kinetic data for wild-type MnSOD (*6*, *8*). We have fitted this more complex scheme to our kinetic data, which increases considerably the number of fitted variables but affirms our conclusions based on the use of the more simplified scheme.[5] For example, application of the more complex scheme estimated that the reverse of eq 4 is smaller by ~100-fold than the forward step k_4 for human wild-type MnSOD as well as the W161A and W161F mutants. In fact, Hearn et al. (*7*) have observed the characteristic visible absorption pattern of the inhibited complex upon mixing Mn(III)SOD and H_2O_2; however, this

[5] For example, comparison of Figures 3 and 4 demonstrates that the formation and dissociation of the product-inhibited complex are well-separated in time under experimental conditions. Hence, the representation of the rate constant for formation of the inhibited complex as $k_3[O_2^{\bullet-}]$ in eq 3 would be represented as $k_3[O_2^{\bullet-}] + k_{-3}$ in the more complex scheme including reverse steps.

result required rather large concentrations of H_2O_2 near 25 mM and is certainly not a factor with the much smaller micromolar levels of substrate used in this work.

Summary. Replacement of the prominent Trp161 forming a hydrophobic side of the active site cavity of human MnSOD has caused significant conformational changes on adjacent residues near the active site, particularly Gln143 and Tyr34 which in the wild type participate in a hydrogen bond network believed to support proton transfer during catalysis. These changes for W161A and W161F MnSOD are associated with a decrease by at least 100-fold in the extent of catalytic reduction of superoxide, which then promotes a competing pathway leading to product inhibition. The rate constant for formation of the product-inhibited complex in H_2O and D_2O changes rather little with these significant structural changes in the mutants, indicating that this formation is largely a function of the metal and does not involve a rate-contributing proton transfer. The rate constant for dissociation of the inhibited complex shows a greater variation among these mutants of MnSOD and has a solvent hydrogen isotope effect indicating a rate-contributing proton transfer. These results are consistent with a mechanism in which the inhibited state is a complex of the peroxide dianion O_2^{2-} with the manganese, the dissociation of which as HO_2^- or H_2O_2 is promoted by proton transfer.

REFERENCES

1. Fridovich, I. (1997) *J. Biol. Chem. 272*, 18515−18517.
2. Bannister, J. V., Bannister, W. H., and Rotilio, G. (1987) *CRC Crit. Rev. Biochem. 22*, 111−180.
3. Holm, R. H., Kennepohl, P., and Solomon, E. I. (1996) *Chem. Rev. 96*, 2239−2314.
4. Cabelli, D. E., Riley, D., Rodriguez, J. A. A., Valentine, J. S., and Zhu, H. (2000) in *Biomimetic Oxidations Catalyzed by Transition Metal Complexes* (Meunier, B., Ed.) Chapter 10, pp 461−508, Imperial College Press, London.
5. McAdam, M. E., Fox, R. A., Lavelle, F., and Fielden, E. M. (1977) *Biochem. J. 165*, 71−79.
6. Bull, C., Niederhoffer, E. C., Yoshida, T., and Fee, J. A. (1991) *J. Am. Chem. Soc. 113*, 4069−4076.
7. Hearn, A. S., Tu, C. K., Nick, H. S., and Silverman, D. N. (1999) *J. Biol. Chem. 274*, 24457−24460.
8. Hsu, J.-L., Hsieh, Y., Tu, C. K., O'Connor, D., Nick, H. S., and Silverman, D. N. (1996) *J. Biol. Chem. 271*, 17687−17691.
9. Fridovich, I. (1986) *Adv. Enzymol. Relat. Areas Mol. Biol. 41*, 35−47.
10. Steinman, H. (1982) in *Superoxide Dismutase* (Oberley, L. W., Ed.) Vol. 1, pp 11−69, CRC Press, Boca Raton, FL.
11. Cabelli, D. E., Guan, Y., Leveque, V., Hearn, A. S., Tainer, J. A., Nick, H. S., and Silverman, D. N. (1999) *Biochemistry 38*, 11686−11692.
12. Borgstahl, G. E. O., Parge, H. E., Hickey, M. J., Beyer, W. F., Hallewell, R. A., and Tainer, J. A. (1992) *Cell 71*, 107−118.
13. Guan, Y., Hickey, M. J., Borgstahl, G. E. O., Hallewell, R. A., Lepock, J. R., O'Connor, D., Hsieh, Y., Nick, H. S., Silverman, D. N., and Tainer, J. A. (1998) *Biochemistry 37*, 4722−4730.
14. Sorkin, D. L., Duong, D. K., and Miller, A.-F. (1997) *Biochemistry 36*, 8202−8208.
15. Edwards, R. A., Whittaker, M. M., Whittaker, J. W., Baker, E. N., and Jameson, G. B. (2001) *Biochemistry 40*, 15−27.
16. Beck, Y., Oren, R., Amit, B., Levanon, A., Gorecki, M., and Hartman, A. J. (1987) *Nucleic Acids Res. 15*, 9076.
17. Carlioz, A., and Touati, D. (1986) *EMBO J. 5*, 623−630.
18. Beck, Y., Bartfeld, D., Yavin, Z., Levanon, A., Gorecki, M., and Hartman, J. R. (1988) *Bio/Technology 6*, 930−935.
19. Buxton, G. V., Greenstock, C. L., Helman, L. P., and Ross, A. B. (1988) *J. Phys. Ref. Data 17*, 678.
20. Schwarz, H. A. (1981) *J. Chem. Educ. 58*, 101−105.
21. Rabani, J., and Nielson, S. O. (1969) *J. Phys. Chem. 73*, 3736−3744.
22. Schowen, K. B., and Schowen, R. L. (1982) *Methods Enzymol. 87*, 551−606.
23. Hsieh, Y., Guan, Y., Tu, C. K., Bratt, P. J., Angerhofer, A., Lepock, J. R., Hickey, M. J., Tainer, J. A., Nick, H. S., and Silverman, D. N. (1998) *Biochemistry 37*, 4731−4739.
24. Otwinowski, Z., and Minor, W. (1997) *Methods Enzymol. 276*, 307−326.
25. McRee, D. E. (1992) *J. Mol. Graphics 10*, 44−47.
26. Leveque, V. J.-P., Stroupe, M. E., Lepock, J. R., Cabelli, D. E., Tainer, J. A., Nick, H. S., and Silverman, D. N. (2000) *Biochemistry 39*, 7131−7137.
27. Ramilo, C. A., Leveque, V., Guan, Y., Lepock, J. R., Tainer, J. A., Nick, H. S., and Silverman, D. N. (1999) *J. Biol. Chem. 274*, 27711−27716.
28. Zimmerle, C. T., and Frieden, C. (1989) *Biochem. J. 258*, 381−387.
29. Vance, C. K., and Miller, A.-F. (1998) *J. Am. Chem. Soc. 120*, 461−467.
30. Whittaker, M. M., and Whittaker, J. W. (1997) *Biochemistry 36*, 8923−8931.
31. Lah, M. S., Dixon, M. M., Pattridge, K. A., Stallings, W. C., Fee, J. A., and Ludwig, M. L. (1995) *Biochemistry 34*, 1646−1660.

BI011047F